Supplementary Information

Biomimetic Manganese-eumelanin Nanocomposites for Combined Hyperthermia-immunotherapy against Prostate Cancer

Yu Liu,[1,2,3,5‡] Wenting Shang,[3‡] Heng Liu,[4‡] Hui Hui[3], Jun Wu[3], Wei Zhang[3], Pengli Gao[1,3,5], Kunxiong Guo[3], and Yanli Guo[2], Jie Tian[1,3,5,6]**

[‡]These authors contributed equally to this work.

Dr. Y. Liu, Dr. P. Gao, Prof. J. Tian

[1]Beijing Advanced Innovation Center for Big Data-Based Precision Medicine, School of Medicine and Engineering, Beihang University, Beijing, 100191, China

Dr. Y. Liu, Prof. Y. Guo

[2]Department of Ultrasound, Southwest Hospital, Army Medical University, Chongqing 400000, China

Dr. W. Shang, Dr. H. Hui, Dr. J. Wu, Dr. W. Zhang, M.M. K. Guo

[3]CAS Key Laboratory of Molecular Imaging, Beijing Key Laboratory of Molecular Imaging, the State Key Laboratory of Management and Control for Complex Systems, Institute of Automation, Chinese Academy of Sciences, Beijing, 100190, China

Dr. H. Liu

[4]Department of Radiology, PLA Rocket Force Characteristic Medical Center, Beijing 100088, China

Dr. Y. Liu, Dr. P. Gao, Prof. J. Tian

[5]Key Laboratory of Big Data-Based Precision Medicine (Beihang University), Ministry of Industry and Information Technology, Beijing, 100191, China
Prof. J. Tian
[6]Engineering Research Center of Molecular and Neuro Imaging of Ministry of Education, School of Life Science and Technology, Xidian University, Xi'an, Shaanxi, 710126, China
Corresponding author: Yanli Guo (guoyanli71@aliyun.com); Jie Tian (jie.tian@ia.ac.cn)

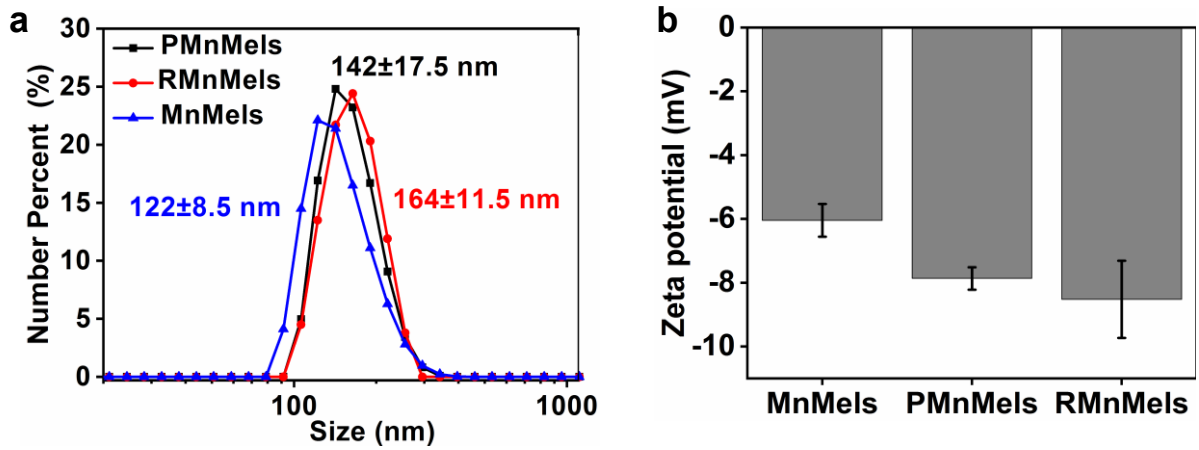

Figure S1. (a) Hydrodynamic sizes of nanoparticles. (b) Zeta potential of nanoparticles.

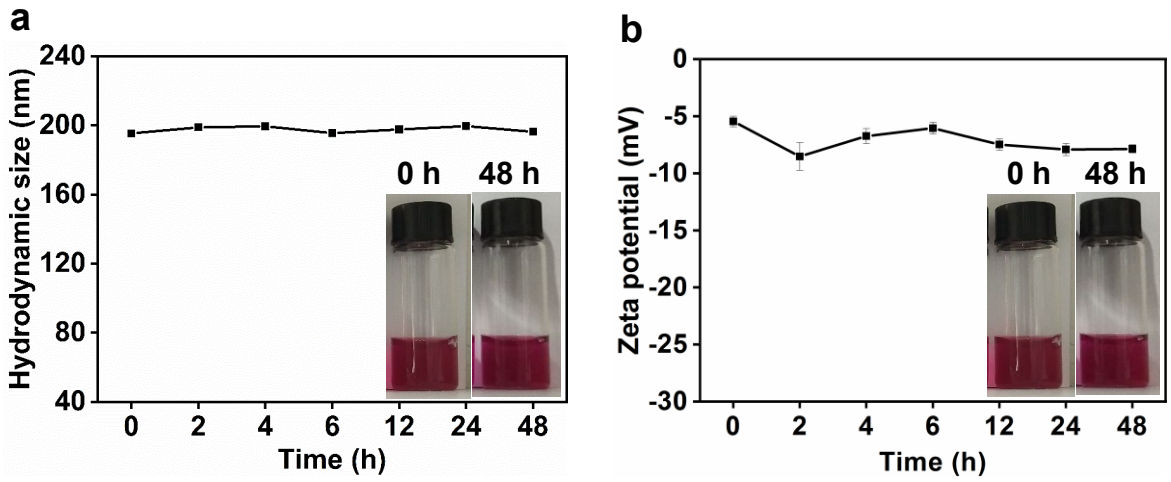

Figure S2. (a) Hydrodynamic size and (b) zeta potential changes of RMnMels solution in DMEM containing 10 % FBS over 48 h. The insets show digital photographs of solutions at 0 h and 48 h.

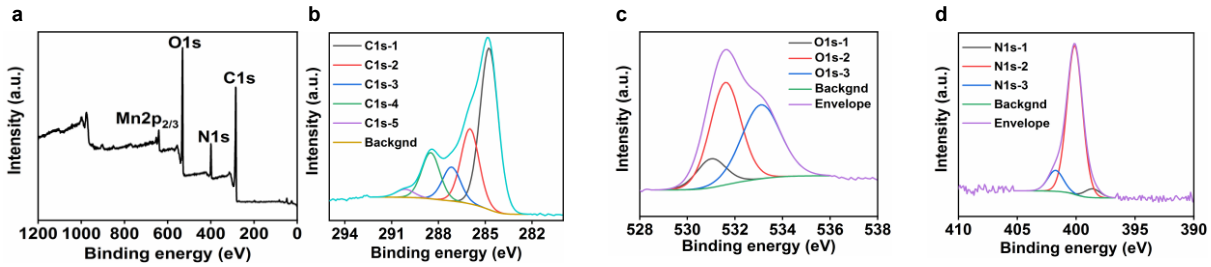

Figure S3. (a) XPS survey spectra. XPS spectra of (b) C1s, (c) N1s and (d) O1s for RMnMels.

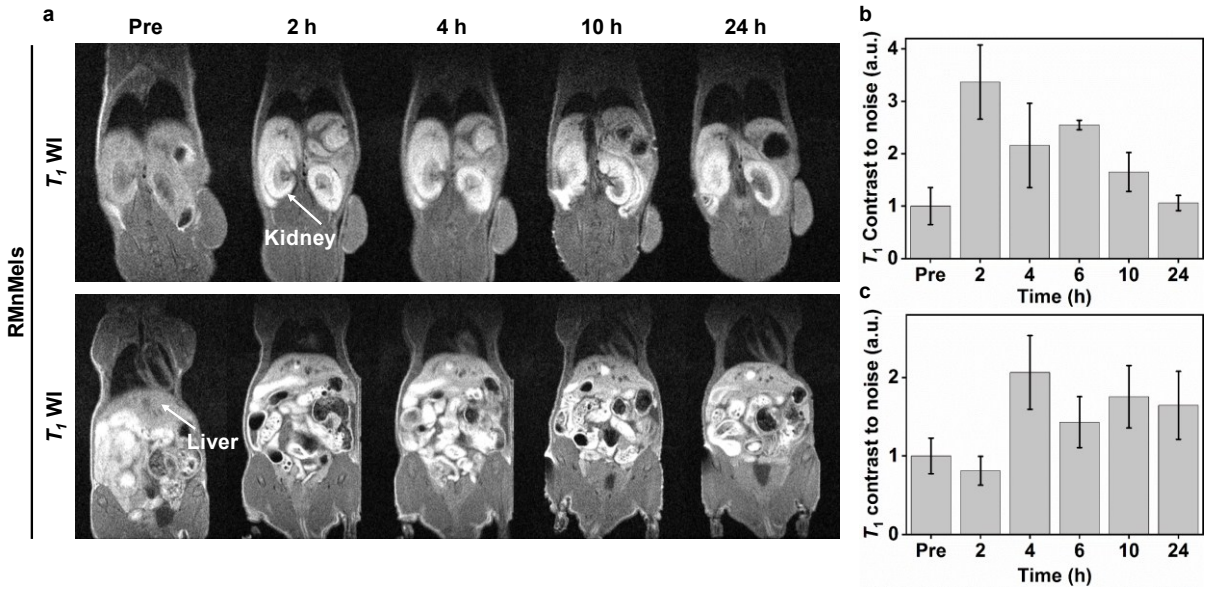

Figure S4. (a) T_1-weighted MR images of mice kidneys and liver prior to and at various time points post intravenous injection of RMnMels at 12mg/kg body weight. The images were acquired at 1.5 T. Normalized signal intensities determined from mice (b) kidneys and (c) liver.

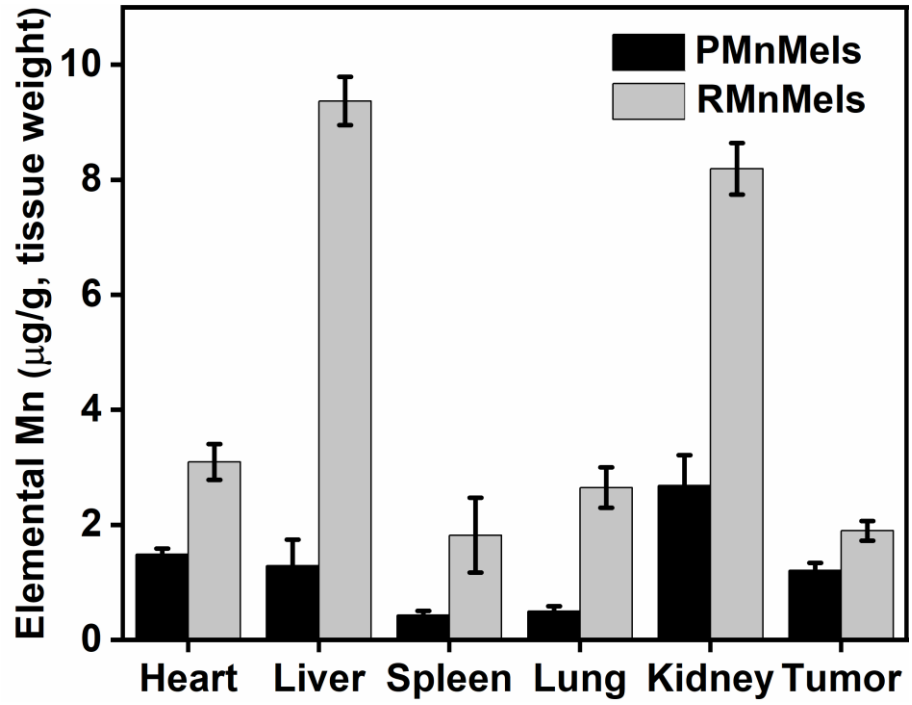

Figure S5. The amount of manganese (Mn) elements per gram of tissue.

Such a substantial signal change was benefitted from peptide mediated active targeting effect. ICP-MS results showed that about 1.9 μg/g (16% i.d./g) of Mn per gram of tumor tissues was delivered by RMnMels at 6 h post injection, while 1.2 μg/g (10% i.d./g) for non-targeted PMnMels (Figure S5)

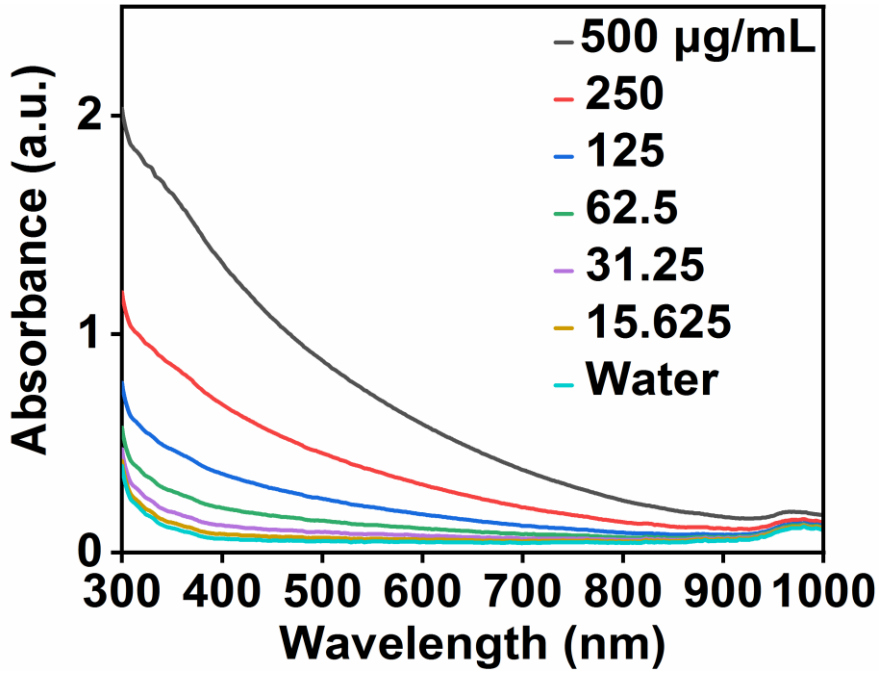

Figure S6. UV-vis absorption profile of RMnMels with various mass concentrations.

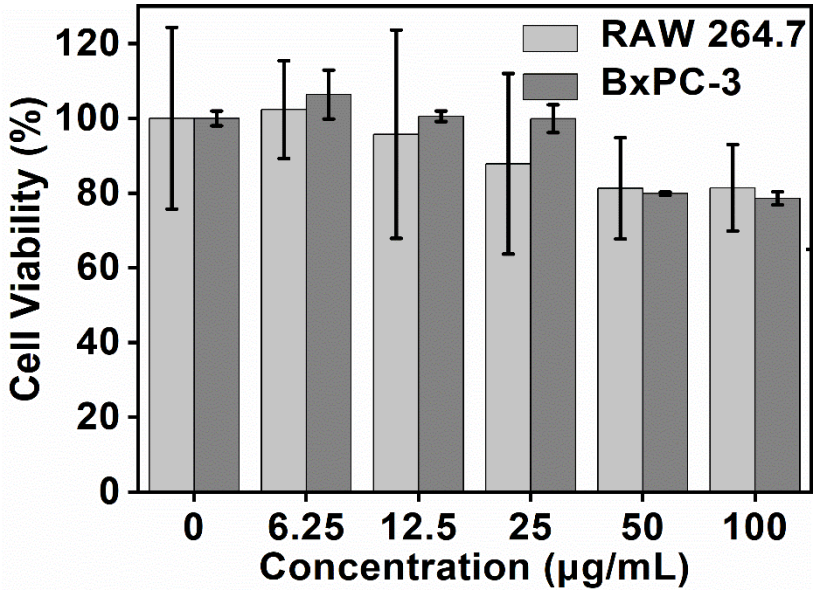

Figure S7. Cell viability of PC3 and RAW 264.7 cells after co-incubation with various concentrations of RMnMels.

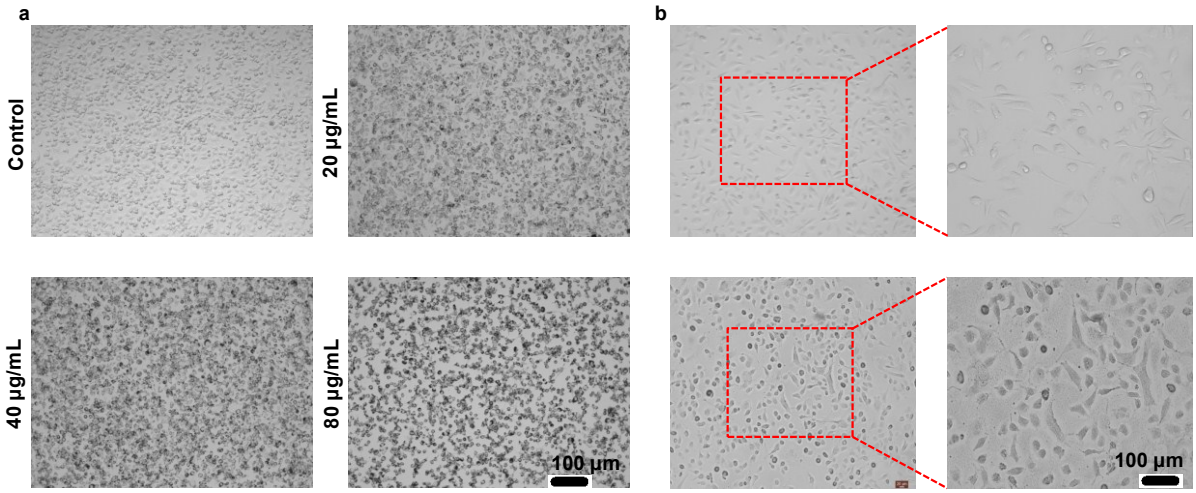

Figure S8. (a) Optical microscope images of RAW 264.7 cells after co-incubation with various concentrations of RMnMels for 12 h. Scale bars, 100 μm. (b) Optical microscope images of PC3 cells after incubation without (upper) or with (lower) 50 μg/mL RMnMels for 12 h. Scale bars, 100 μm.

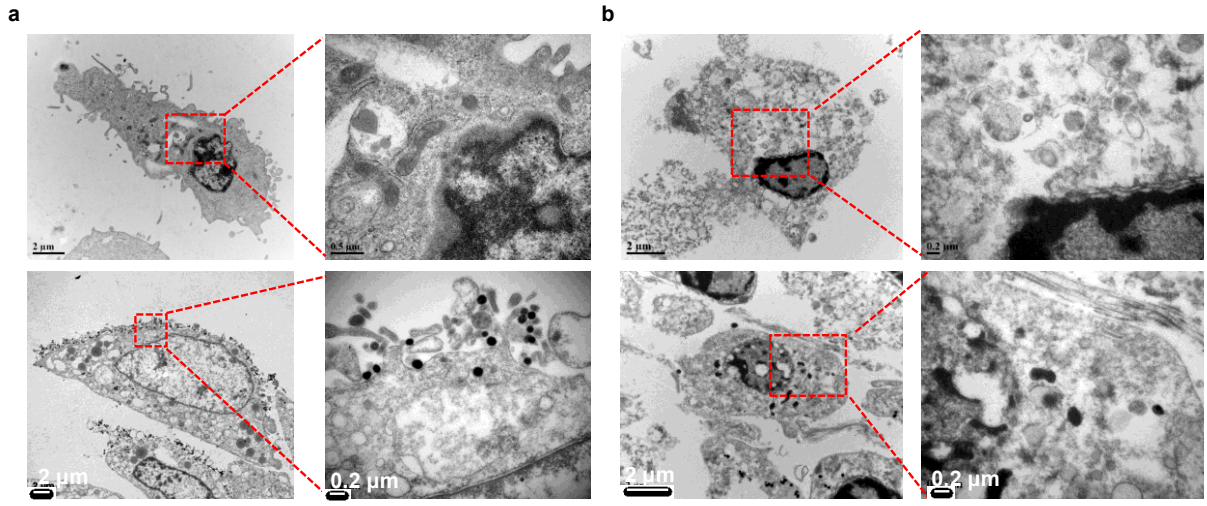

Figure S9. (a) Cellular TEM images of PC3 cells after incubation without (upper) or with (lower) RMnMels at 50 μg/mL for 12 h. (b) Tissue TEM images of PC3 tumor tissue slices after intravenous injection of PBS (upper) or RMnMels (lower) for 48 h.

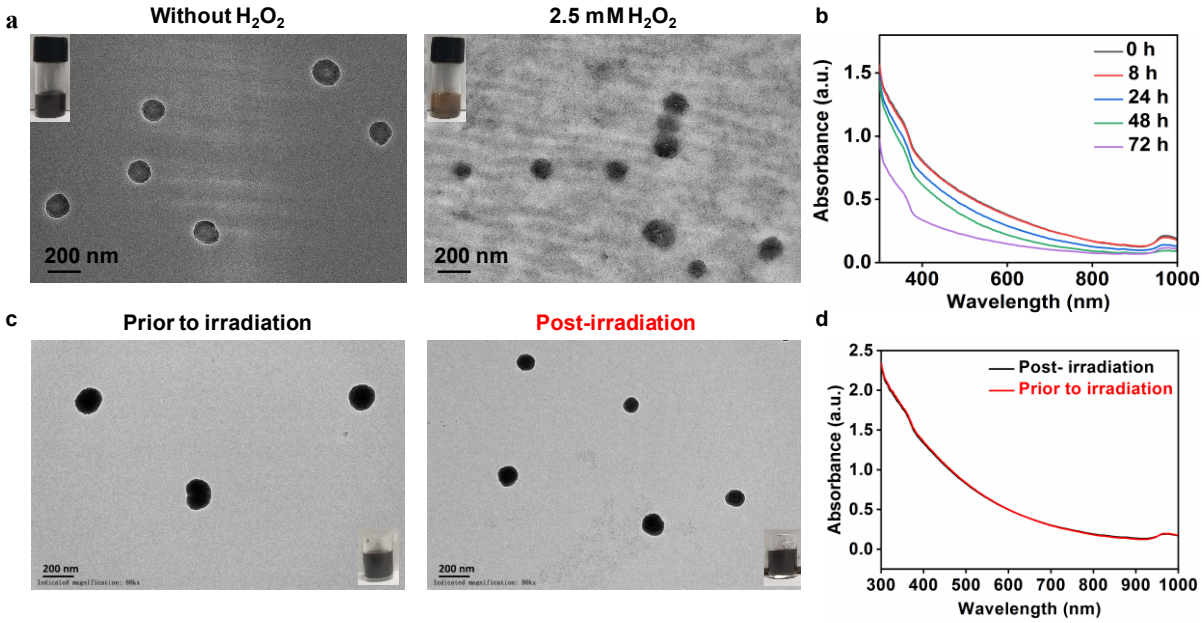

Figure S10. (a) TEM images of RMnMels with/without 2.5 mM H_2O_2 for 72 h. Scale bar, 200 nm. The insets show corresponding digital photographs. (b) UV-vis absorption spectra of RMnMels co-incubation with 2.5 mM H_2O_2 at different time points. (c) TEM images of RMnMels solution before and after 690 nm laser irradiation (500 mW/cm^2, 30 min). Scale bar, 200 nm. The insets show corresponding digital photographs. (d) UV-vis absorption spectra of RMnMels aqueous solutions prior to and after exposure to 690 nm laser irradiation.

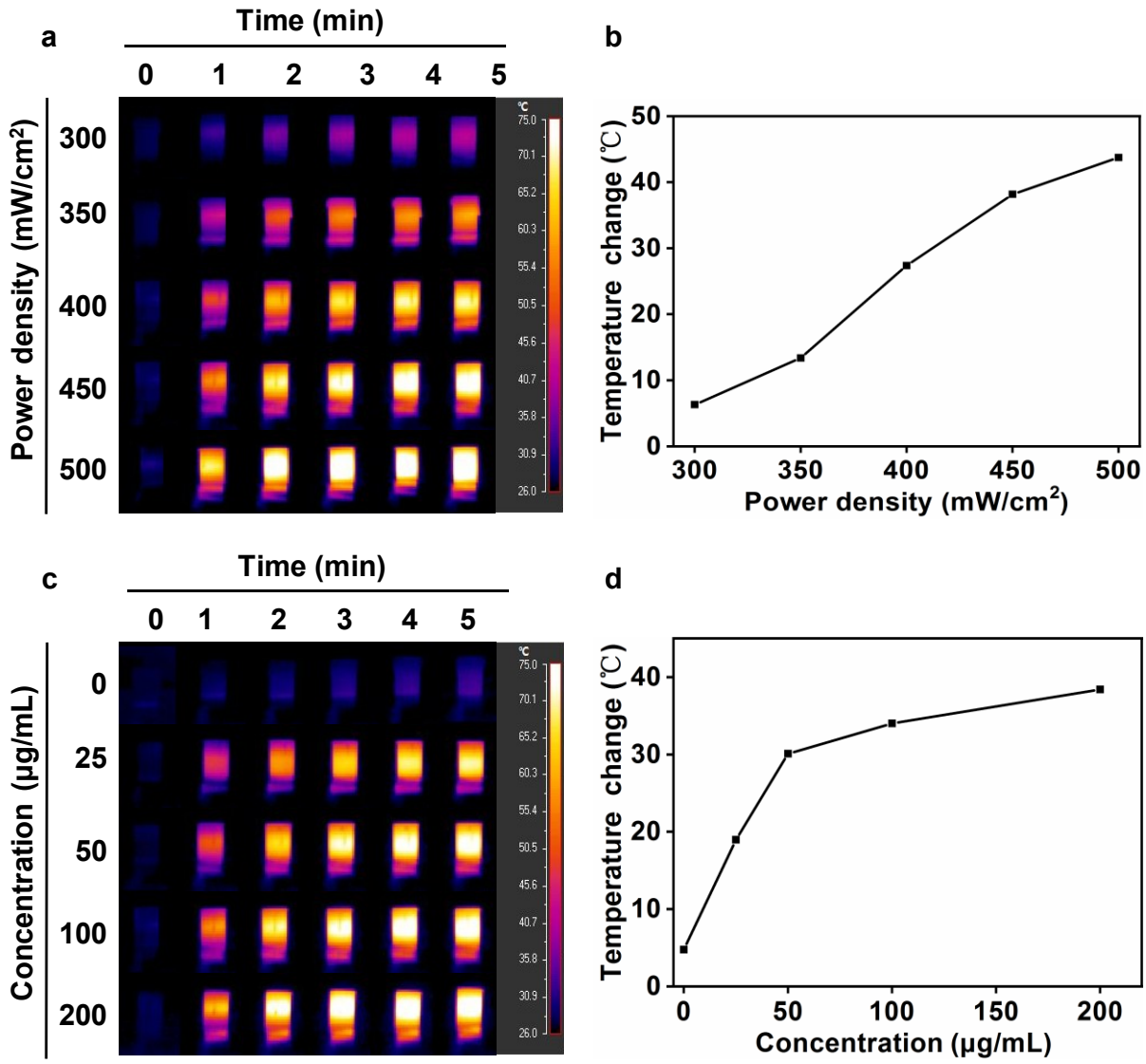

Figure S11. (a) Infrared thermal images and (b) temperature variations of 200 μg/mL RMnMels aqueous solution during exposure to a 690 nm laser with different power densities for 300 s. (c) Infrared thermal images and (d) temperature variations of RMnMels aqueous solution with different concentrations during exposure to a 690 nm laser at 500 mW/cm^2 for 300 s.

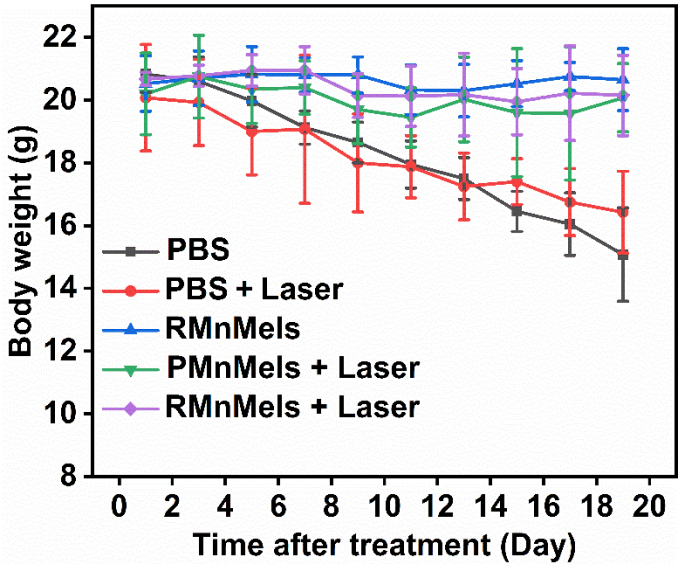

Figure S12. (a) body weight curves of mice during a period of 19 days after different treatments.

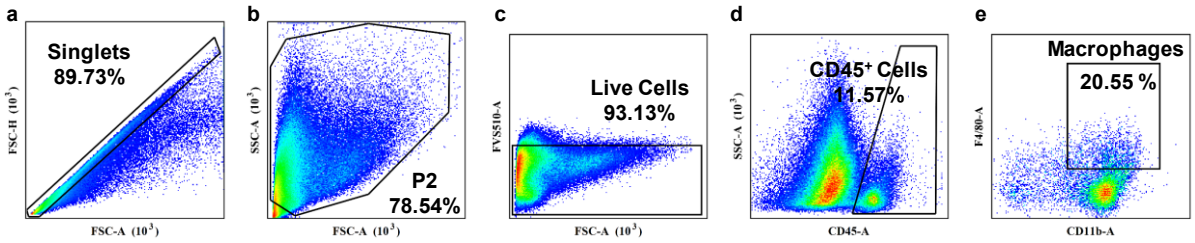

Figure S13. Flow cytometry analysis of tumor immune cells. Gating strategy showing delineation of (a) singlets cells. (b) Numbers indicate the percentages of the cells within the gates. (c) Live Cells. (d) $CD45^+$ leukocytes. (e) Tumor-associated macrophage.

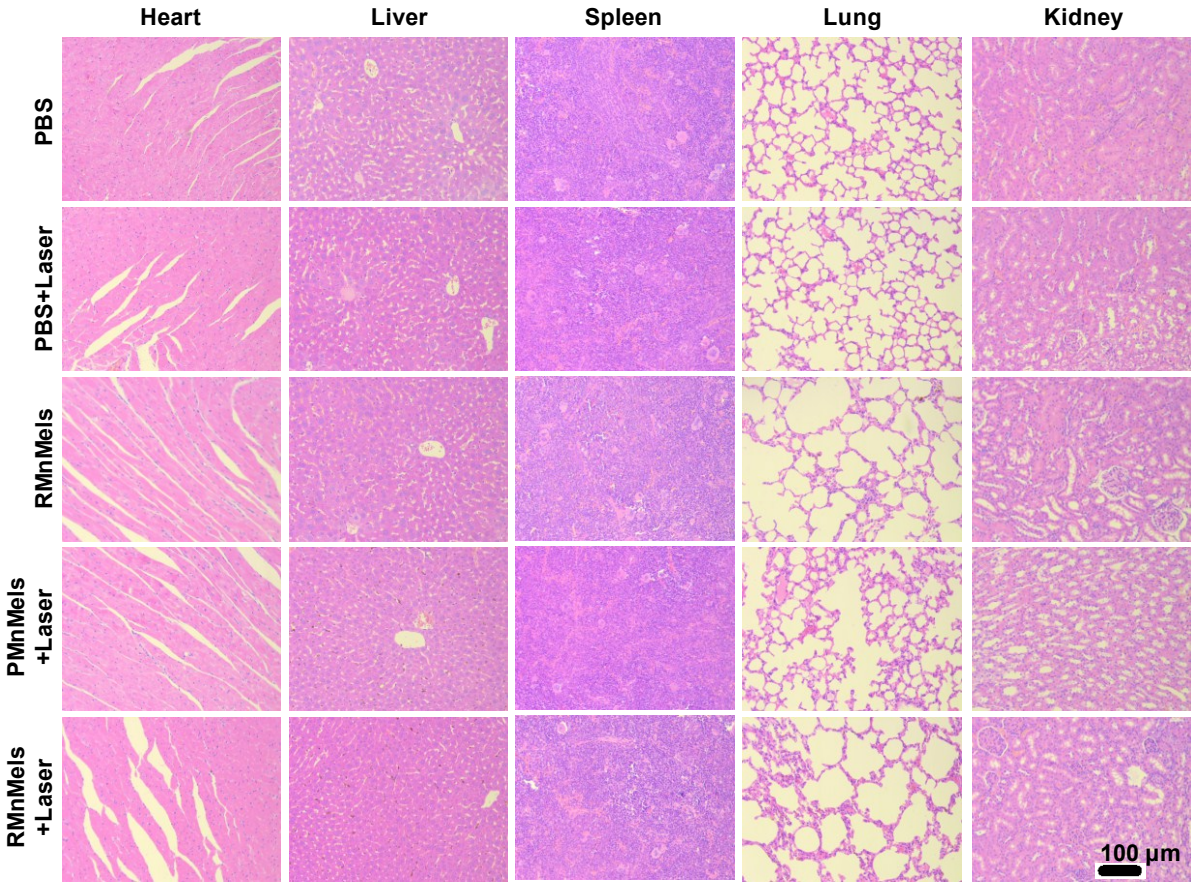

Figure S14. H&E stained images of mice major organ sections on day 19 after different treatments. Scale bar, 100 μm.

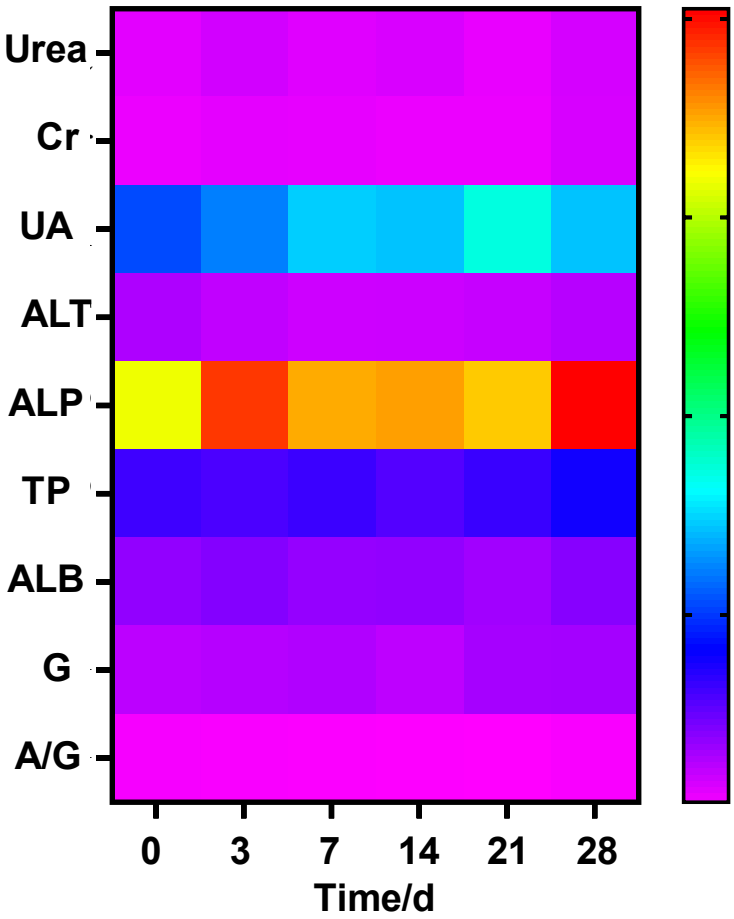

Figure S15. Serum biochemical indexes of healthy mice obtained on different time point.

Table S1 Primer sequences for different genes.

Gene name	Forward primer	Reverse primer
TNF-α	TCCCCAAAGGGATGAGAAGTT	GAGGAGGTTGACTTTCTCCTGG
CD86	CTAAGCAAGGTCACCCGAAAC	GGCCACAGTAACTGAAGCTGTAT
iNOS	CATTCAGATCCCGAAACGCT	TGTAGGACAATCCACAACTCGC
CD206	AGCTGCTGTCGCTGGAAT	GGATGCTTGAGAAGTGAATAGG
Arginase-1	TGTGGGAAAAGCCAATGAA	GGTGTCAGCGGAGTGTTG
GAPDH	TGAAGGGTGGAGCCAAAAG	AGTCTTCTGGGTGGCAGTGAT